# Stability Modeling and Comparative Study of Series Vectorial Compensators

J. Miguel González, *Student Member, IEEE,* Claudio A. Cañizares, *Fellow, IEEE,* and Juan M. Ramírez, *Member, IEEE*

***Abstract*—Complete stability analyses, including voltage, small perturbation and transient stability studies, and the associated models and controls of a Series Vectorial Compensator (SVeC) are presented in this paper. A full comparative evaluation of this controller with respect to controllers used mainly for oscillation control in transmission corridors, namely, Thyristor-Controlled Series Capacitors (TCSC) and Series Static Synchronous Compensators (SSSC), is presented for the first time. The IEEE 14-bus benchmark system and a 190-bus, 46-machine model of the Mexican grid are used for illustrative and comparison purposes. The results obtained show that the SVeC has better oscillation damping characteristics than the TCSC and SSSC, hence making these types of controllers a competitive alternative against existing series Flexible AC Transmission System (FACTS) controllers for dynamic series compensation of transmission lines, especially where space and cost are an issue.**

***Index Terms*—Flexible AC Transmission System (FACTS), Series Vectorial Compensator (SVeC), Series Static Synchronous Compensator (SSSC), Thyristor-Controlled Series Capacitor (TCSC), voltage stability, small-perturbation stability, transient stability, power oscillation control, Hopf bifurcations.**

## I. Glossary of Terms

| | |
|---|---|
| DAE: | Differential Algebraic Equations. |
| FACTS: | Flexible AC Transmission Systems. |
| HB: | Hopf bifurcation. |
| ODAE: | Ordinary Differential Algebraic Equations |
| POD: | Power Oscillation Damping. |
| PSS: | Power System Stabilizer. |
| PWM: | Pulse Width Modulation. |
| TCSC: | Thyristor-Controlled Series Capacitor. |
| TCR: | Thyristor-Controlled Reactor. |
| SVeC: | Series Vectorial Compensator. |
| SSSC: | Series Static Synchronous Compensator. |
| STATCOM: | Shunt Static Synchronous Compensator. |
| SVC: | Static Var Compensator. |
| UPFC: | Unified Power Flow Controller. |
| VSC: | Voltage-Sourced Converter. |

## II. Introduction

This paper was submitted on November 2008. Revised and resubmitted on April 2009. Accepted May 2009.

This work was supported by CONACyT, Mexico and the Natural Sciences and Engineering Research Council (NSERC) of Canada.

Juan Miguel Gonzalez and Juan Manuel Ramirez are with CINVESTAV, Guadalajara, Jalisco, CP 45010, Mexico (email: jramirez@gdl.cinvestav.mx).

Claudio A. Canizares is with the Department of Electrical and Computer Engineering, University of Waterloo, Waterloo, ON, N2L 3G1, Canada (email:ccanizar@uwaterloo.ca).

POWER systems are currently operating closer to their static and dynamic stability limits due to an increase in the power transfer demands on existing transmission systems, given the significant growth of loads and generation, lack of new transmission lines, and competitive electricity market pressures. Stability problems associated with voltage collapse and undamped oscillations are currently the leading causes of major blackouts (e.g. [1], [2]). In this context, FACTS controllers are becoming more relevant, since due to their fast response, these controllers can improve the stability of a power system, thereby allowing a more efficient use of existing transmission grids [3].

Various types of FACTS controllers, particularly SVCs, TCSCs, STATCOMs, SSSCs and UPFCs are being used in practice [3]–[7], some more than others; for example, in Brazil, TCSCs are used as an alternative to PSSs for the control of inter-area power oscillations in a North-South interconnection [8]. These controllers are based on thyristors or VSC-based converters. However, more recently, new controllers based on ac-ac vectorial converters have been proposed [9]–[14], demonstrating that it is possible to attain similar control objectives and performance as those based on VSC converters; in all these papers, as opposed to the present paper, detailed switching models rather than stability models of the vectorial converters are used for simulation purposes. Thus, in [9], the authors discuss the use of an SVeC to control active power on a transmission line with a simple structure, injecting a series capacitive reactance that is adjusted automatically through a duty cycle control. A brief comparison of the SVeC with respect to a TCSC is presented in [10] on a small radial power system with three buses, a generator and a load, showing that the SVeC presents a smoother control alternative than the TCSC during transients, since the TCSC is designed to "jump" from capacitive to inductive operating regions in transient operating conditions to avoid open-circuit operation and to reduce harmonics [15].

A comparative evaluation between the SVeC and an SSSC is presented in [14], based on detailed switching models and a single generator-infinite bus (SIB) test system, showing that the dc-link requires about twice as much capacitive energy storage and about 66% additional semiconductor MVA rating for the same application. No practical SVeC has been built and installed on a real transmission system thus far; however, a comparative estimate of components' costs for these two controllers is presented in [14], based on publicly available information regarding costs of transformers and capacitors, and power-semiconductor manufacturers' quotes.

The aforementioned paper shows that the cost of the SSSC is higher than the SVeC, with the latter presenting higher losses. It is also mentioned that the SVeC can operate at higher temperatures due to the use of ac capacitors as opposed to the dc capacitors used in the SSSC, which are quite vulnerable to high temperatures. Finally, it is argued that another advantage of the SVeC's converter topology is its more compact size compared to the SSSC's VSC converter. Similar arguments are presented in [16] and [17].

Based on the aforementioned comparisons, it can be argued that direct PWM, vectorial-converter-based controllers may be a reasonable alternative to thyristor- and VSC-based options for similar applications. Therefore, it is necessary to perform further comparative studies between converter technologies for the same power system applications to determine all possible SVeC's advantages and disadvantages with respect to TCSC and SSSC series controllers; this is the main focus of the present paper. Thus, this paper concentrates on performing detailed comparative voltage, transient and oscillatory stability studies, as well as proposing and discussing the required SVeC models and controls for these types of studies, considering this controller's application and performance in multi-machine power systems.

The current authors have presented in [18]–[20] some studies of the effect of an SVeC on power system stability. Thus, the controller steady-state performance is analyzed in [18], based on a power flow model of the SVeC. Some transient stability studies are discussed in [19] and [20], based on a somewhat complex stability model and a simple control approach for active power regulation; in these papers, it is shown that the controller does not provide enough damping for certain contingencies. Based on these preliminary studies, besides the comparative studies with respect to TCSCs and SSSCs for overall stability improvement presented here, a better and simpler stability model and POD control for the SVeC is proposed and studied in the present paper.

The rest of the paper is structured as follows: Section III explains briefly the basic background theory behind the models and analysis approach used in the current paper, presenting a brief discussion of DAE power system models, small-perturbation stability studies and HBs. Previously proposed and widely used TCSC and SSSC stability models and their controls, including POD controls, are presented and discussed in this section as well. Section IV describes in detail the proposed SVeC stability model and its controls. Complete stability studies and associated results obtained for the IEEE 14-bus benchmark system and a 190-bus, 46-machine model of the Mexican power system, including the 3 different FACTS controllers under study, are shown and discussed in Section V. A summary and the main contributions of the paper are presented in Section VI.

## III. Background

### A. Small-perturbation Analysis and P-V curves

In general, power systems are modeled using a set of DAE equations as follows:

$$\dot{x} = f(x, y, \lambda, p) \tag{1}$$

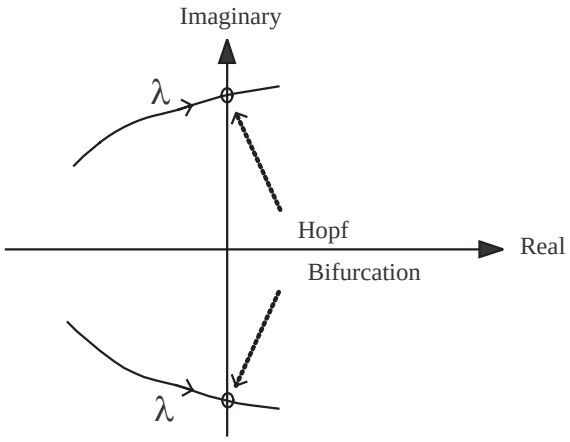


Fig. 1. Locus of the critical eigenvalues as a system parameter $\lambda$ changes.

$$0 = g(x, y, \lambda, p)$$

where $x \in \Re^n$ is a vector of state variables associated with the dynamic states of generators, loads, and other system controllers, such as FACTS compensators; $y \in \Re^m$ is a vector of algebraic variables associated with steady-state models of loads and transmission system components; $\lambda \in \Re^l$ a set of uncontrollable parameters such as variations in active and reactive power of loads; $p \in \Re^k$ is a set of controllable parameters such as controllers' set points; $f(\cdot)$ is the set of differential equations associated with the state variables $x$; and $g(\cdot)$ is the set of algebraic equations associated with the algebraic variables $y$.

Bifurcation analyses are based on steady state studies [21], which include eigenvalue or small-perturbation stability analyses of power systems [22], as some system parameters $\lambda$ and/or $p$ change in (1) [23]. These studies are based on the eigenvalues of the system Jacobian $J$ in the following linearization of (1):

$$\begin{bmatrix} \Delta\dot{x} \\ 0 \end{bmatrix} = \begin{bmatrix} J_1 & J_2 \\ J_3 & J_4 \end{bmatrix} \begin{bmatrix} \Delta x \\ \Delta y \end{bmatrix} \tag{2}$$

where $J_1 = \partial f/\partial x|_0$, $J_2 = \partial f/\partial y|_0$, $J_3 = \partial g/\partial x|_0$ , $J_4 = \partial g/\partial y|_0$ . If $J_4$ is non-singular, the system eigenvalues can be readily computed by eliminating the vector of algebraic variable $\Delta y$ in (2), i.e.,

$$\Delta\dot{x} = \left(J_1 - J_2 J_4^{-1} J_3\right) \Delta x = A\Delta x \tag{3}$$

Thus, the DAE system is basically reduced to a set of ODE equations [24]. Bifurcations on power system models can then be detected by monitoring the eigenvalues of matrix $A$ in (3) as the system parameters $(\lambda, p)$ change. In practice, the eigenvalues of $A$ are obtained directly from the system Jacobian $J$, since this matrix is sparse, whereas $A$ is full [22].

PV curves are typically used for voltage stability studies of power systems [23], and if these are combined with eigenvalue analyses, they can also be used as a means to understand oscillatory stability [25]. The maximum loadability points in these curves, which are typically obtained by means of

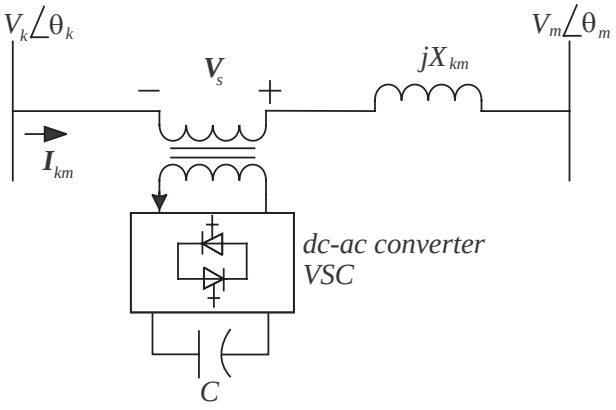


Fig. 2. SSSC single-line diagram.

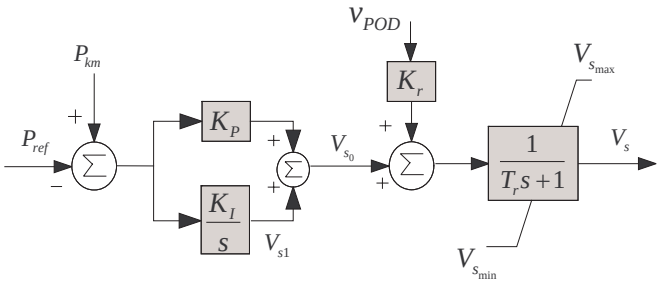


Fig. 3. SSSC power regulator.

continuation power flows, can be associated with voltage collapse instabilities.

In general, voltage collapse and oscillatory phenomena have been associated with bifurcation phenomena in nonlinear systems. Therefore, bifurcation theory has been used in, for example, [25]–[29] to study oscillation problems and design corrective controls for damping these oscillations in power systems; in these papers, HBs are linked to oscillatory instabilities.

HBs are characterized by periodic orbits emerging around an equilibrium point [21], and can be studied with the help of eigenvalue analyses. At a HB point, the system model (1) presents a pair of purely imaginary eigenvalues of the state matrix $A$ in (3) as the $(\lambda, p)$ parameters change [25]; thus, the point where a complex conjugate pair of eigenvalues cross the imaginary axis as the system parameters $\lambda$ and/or $p$ change is known as a HB point, as illustrated in Fig.1.

Since, as mentioned above, HBs can be associated with small active power oscillations in power systems [25]–[29], series-connected FACTS controllers with active power controls have been proposed and are being used for the control of inter-area oscillations [3], [8], [15]. Hence, the following sections concentrate on describing and discussing typical active power linear controls used for damping small power oscillations in these types of FACTS controllers, i.e. SSSC, TCSC and SVeC.

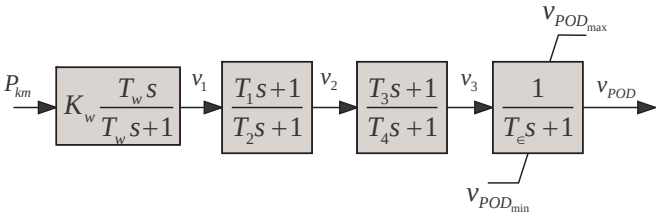


Fig. 4. POD control block diagram.

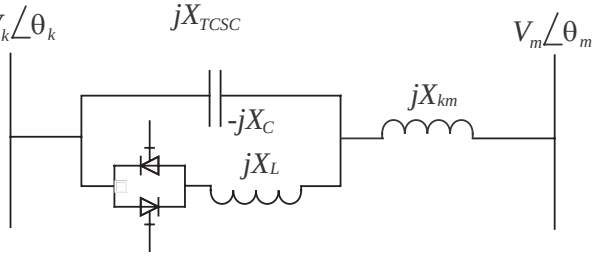


Fig. 5. TCSC single-line diagram.

### B. SSSC Model and Controls

The SSSC is based on a VSC device that injects a voltage in series with the transmission line. The transient stability model used in this paper is extracted from [30], where the SSSC is represented by a series-connected voltage phasor source $\mathbf{V}_S$, as depicted in Fig.2, which is always kept in quadrature with the line current phasor $\mathbf{I}_{km}$, so that the SSSC can exchange only reactive power with the system. Thus, the controllable parameter in this case is the magnitude $V_S$, which is used to regulate active power flow. This model yields the following algebraic power flow equations between the $k$ and $m$ nodes in Fig.2:

$$\begin{aligned} P_{km} &= (1+\Psi)\, V_k V_m B_{km} \sin(\theta_k - \theta_m) \\ P_{mk} &= -P_{km} \\ Q_{km} &= (1+\Psi)\, V_k B_{km} \left[V_k - V_m \cos(\theta_k - \theta_m)\right] \\ Q_{mk} &= (1+\Psi)\, V_m B_{km} \left[V_m - V_k \cos(\theta_k - \theta_m)\right] \end{aligned} \tag{4}$$

where $\Psi = V_s / \sqrt{V_k^2 + V_m^2 - 2V_k V_m \cos(\theta_k - \theta_m)}$, and $V_k\angle\theta_k$, $V_m\angle\theta_m$, and $B_{km} = 1/X_{km}$ are defined in Fig.2.

The basic control strategy in Fig.3 is adopted here to regulate the active power flow. Since the main aim of this SSSC model is to control the active power through the transmission line where is embedded, a $v_{POD}$ input signal is used in its control to damp power oscillations. This signal comes from the POD control depicted in Fig.4, which basically has the same control structure as a typical PSS [22].

### C. TCSC Model and Control

The TCSC transient stability model used here is extracted from [31], and corresponds to a typical TCSC controller based on a TCR in parallel with a bank of capacitors, as depicted in Fig.5. The TCSC can be adequately represented in stability studies by an equivalent reactance $X_{TCSC}$, the value of which

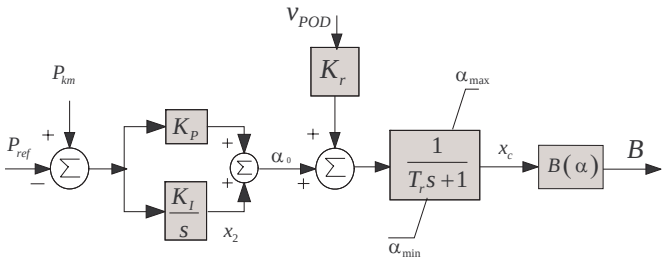


Fig. 6. TCSC power regulator.

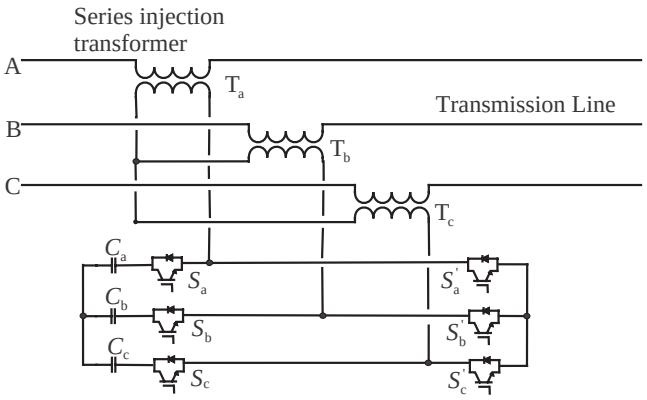


Fig. 7. Transmission line with PWM SVeC.

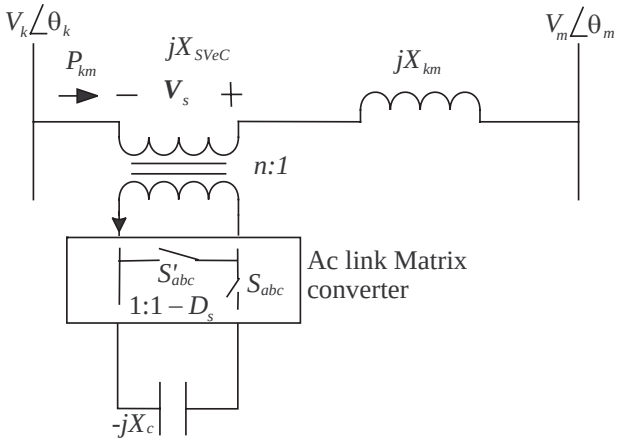


Fig. 8. SVeC single-line diagram.

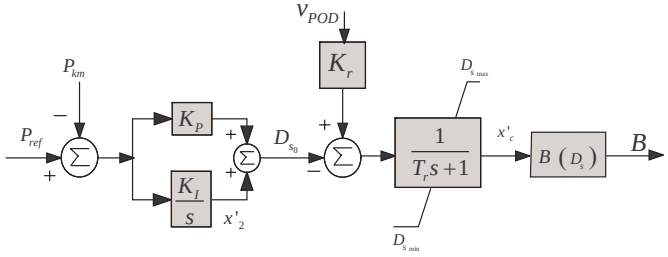


Fig. 9. SVeC power regulator.

is adjusted automatically to regulate the power flow through the transmission line. The variable equivalent reactance of the TCSC controller is allowed to change in either the inductive or the capacitive regions, avoiding the resonance region.

The algebraic equations for the power flows between the $k$ and $m$ nodes associated with this model are the same as those presented in (4), where all phasor voltages are defined in Fig.5. Here, $\Psi$ is function of the thyristors' firing angle [31] as follows:

$$\Psi(\alpha)=\frac{B(\alpha)}{B_{km}} \tag{5}$$

where:

$$B(\alpha)=\frac{\pi\left(k_x^4-2k_x^2+1\right)\cos[k_x(\pi-\alpha)]}{X_{den}} \tag{6}$$

$$\begin{aligned} X_{den}=&X_C\cos[k_x(\pi-\alpha)] \\ &(\pi k_x^4-\pi-2k_x^4\alpha+2k_x^2\alpha-k_x^4\sin(2\alpha)) \\ &+X_C\cos[k_x(\pi-\alpha)]\left(k_x^2\sin(2\alpha)-4k_x^2\cos(\alpha)\sin(\alpha)\right) \\ &-X_C\left[4k_x^3\cos^2(\alpha)\sin[k_x(\pi-\alpha)]\right] \end{aligned} \tag{7}$$

and $k_x=\sqrt{X_C/X_L}$. Note that $X_{TCSC\,\max}$ corresponds to $\alpha_{\max}$, and similarly for the relationship between $X_{TCSC\,\min}$ and $\alpha_{\min}$.

The control strategy depicted in Fig.6 is used here, where $B(\alpha)$ is defined in (6). As is typical in TCSC controllers, the power oscillation damping control illustrated in Fig.4 is also included.

## IV. Series Vectorial Compensator

### A. Description

The schematics of the SVeC are shown in Fig.7 [10]. The series compensator consists of: series injection transformers $T_a$, $T_b$ and $T_c$; compensation capacitors $C_a$, $C_b$ and $C_c$; and PWM-controlled switches $S_a$, $S_b$, $S_c$, $S'_a$, $S'_b$, and $S'_c$. During the period when the switches $S_a$, $S_b$, and $S_c$ are closed, the compensation capacitors are connected. The switches $S'_a$, $S'_b$, and $S'_c$ operate complementarily with respect to $S_a$, $S_b$, and $S_c$, thus avoiding the short-circuiting of the capacitor. In Fig.8, the single-line diagram associated with Fig.7 is depicted; here, the switches $S_a$, $S_b$, $S_c$, $S'_a$, $S'_b$, and $S'_c$ are represented by $S_{abc}$ and $S'_{abc}$, respectively.

The main differences between the SVeC and the TCSC and SSSC controllers are the following:

- *Protection*: In the case of sudden surges, low-pass filters in the SSSC and SVeC help with blocking high frequency voltages and currents associated with the surge. In addition to these filters, the switches are protected against large surges with Metal Oxide Varistors (MOVs). Furthermore, to protect these controllers against overcurrents due to nearby short circuits, the controls are designed to drive the output voltage towards zero in microseconds, so that the power in the controllers during the faults are practically zero, in spite of the high currents. In the case of the TCSC, it is necessary to wait for the next current zero crossing to initiate control action.

- *Number of Switches*: For the minimal three-phase configuration, the TCSC requires six thyristors, while the SSSC and SVeC each need six IGBTs/GTOs, for an optimized SVeC configuration based on two switches per phase as shown in Fig.7.
- *Controls*: To modify the firing angle of the thyristors, the TCSC requires several milliseconds, due to the need for current zero crossings. On the other hand, the SSSC and SVeC controllers can change the switches' duty cycle in hundreds of microseconds; however, a response delay can be introduced through filters. Furthermore, for PWM control, the SSSC requires a synchronous type PWM, which is not the case for the SVeC; this leads to a greater complexity in the SSSC control infrastructure.

The compensator basically provides a variable series reactance $X_{SVeC}$ adjusted through variations of the duty cycle $D_s$. As in the case of the SSSC and TCSC discussed above, this controller is assumed to control the power flow in the line by means of varying its equivalent reactance $X_{SVeC}$ through the control illustrated in Fig.9, as explained in more detail below.

### B. Model and Control

As briefly discussed in Section II, the authors present in [18]–[20] some preliminary steady-state and transient stability studies of the SVeC. In these papers, the models used are based on complex equations that lead to some convergence problems during the numerical studies. Furthermore, a simple PI controller is used in these papers to control the active power through the transmission line, which does not provide adequate damping for all power oscillations triggered by system contingencies. Therefore, a simpler stability model that does not present numerical problems is used here, together with the improved control shown in Fig.9 for the regulation and oscillation damping of the transmission line's active power.

From Fig.8, the equivalent impedance between the sending and receiving end of the SVeC-transmission-line system can be defined as:

$$X_{eq} = X_{km} + X_{SVeC} \tag{8}$$

where, from [10]:

$$X_{SVeC} = -n^2 \left(1 - D_s\right)^2 X_c \tag{9}$$

Observe in (8) and (9) that the effective impedance depends on the duty cycle $D_s$ of the switches; hence, this duty cycle provides a means of realizing the desired power flow control, as depicted in Fig.9. Notice in this figure that, following a similar transient stability modeling approach as in the case of the TCSC, the susceptance $B = B_{km}{-}B_{eq} = 1/X_{km}{-}1/\left(X_{km} + X_{SVeC}\right)$ is assumed to be controlled either directly or indirectly through the duty cycle $D_s$, and the $v_{POD}$ signal comes from the same POD control depicted in Fig.4.

The voltage phasor on the primary (transmission-line) side of the coupling transformer in Fig.8 may be calculated as follows:

$$\mathbf{V}_s = n^2 \left(1 - D_s\right)^2 \mathbf{I}_{km} \tag{10}$$

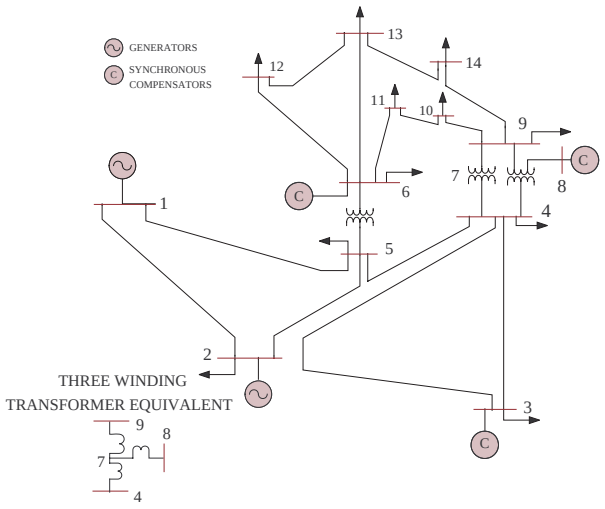


Fig. 10. IEEE 14-bus benchmark test system.

Observe in (8)-(10) that all the quantities are at their maximum value when the duty cycle is zero. Hence, the operating point at minimum duty cycle determines the rating of the converter elements, including the MVA rating of the transformer.

The equations for the power flows associated to the nodes $k$ and $m$ are as follows:

$$\begin{aligned} P_{km}&{=}V_k V_m \left(B_{km} + B\right) \sin\left(\theta_k - \theta_m\right) \\ P_{mk}&{=}{-}P_{km} \\ Q_{km}&{=}V_k^2 \left(B_{km} + B\right) - V_k V_m \left(B_{km} + B\right) \cos\left(\theta_k - \theta_m\right) \\ Q_{mk}&{=}V_m^2 \left(B_{km} + B\right) - V_k V_m \left(B_{km} + B\right) \cos\left(\theta_k - \theta_m\right) \end{aligned} \tag{11}$$

where, from Fig.9:

$$B\left(D_s\right) = -\frac{n^2 \left(1 - D_s\right)^2 X_c}{X_{km}\left[X_{km} - n^2 \left(1 - D_s\right)^2 X_c\right]} \tag{12}$$

Note that this model is much simpler to that proposed in [18]–[20]. From (9), $X_{SVeC\,\min} = -n^2 X_c$, and $X_{SVeC\,\max} = 0$, since $D_{s\,\max} = 1$ and $D_{s\,\min} = 0$.

## V. Results

This section presents and discusses the results obtained from the application of the aforementioned FACTS series controllers for oscillation control to the IEEE 14-bus benchmark system and a 190-bus realistic equivalent of the Mexican power grid. All presented results were obtained with the help of PSAT [31].

### A. IEEE 14-bus Test System

A single-line diagram of the IEEE 14-bus benchmark system described in [31] is shown in Fig.10. It consists of 5 generators, three of which are synchronous compensators used only for reactive power support, all modeled using subtransient stability models and IEEE Type 1 exciters and voltage regulators; 3 transformers; 14 buses; 21 lines; and

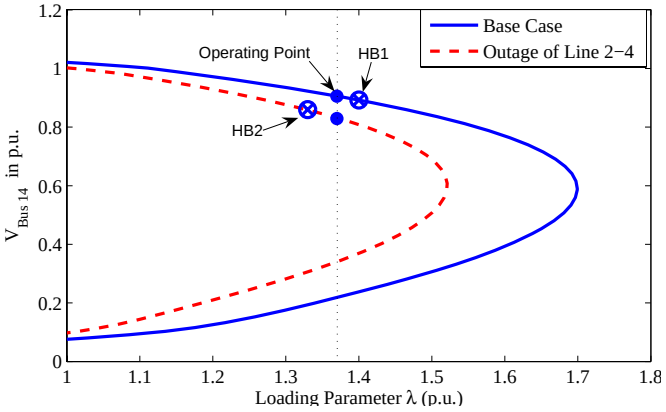


Fig. 11. PV curves for the 14-bus test system.

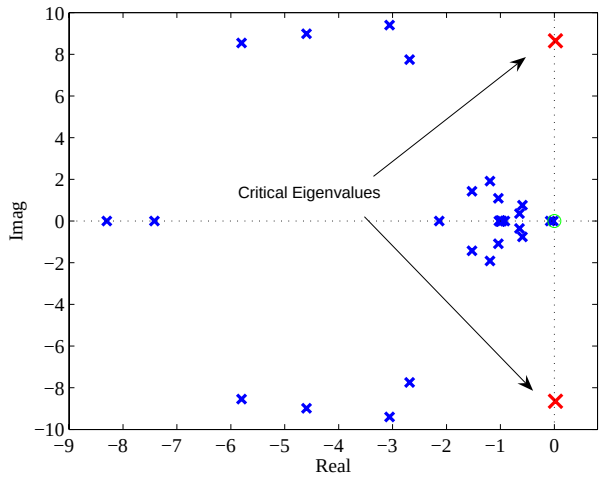


Fig. 12. Eigenvalues for the 14-bus test system for a Line 2-4 outage at $\lambda = 1.4$ p.u.

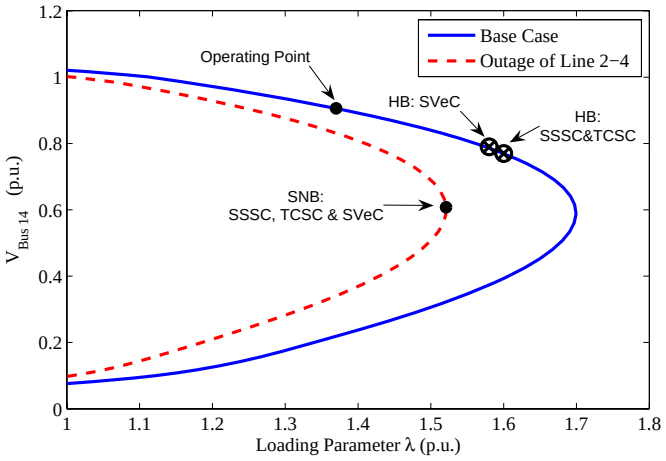


Fig. 13. PV curves for the 14-bus test system with FACTS.

11 loads modeled as constant power loads for maximum system stress. Voltage stability, small-perturbation stability and transient stability studies were performed for the following system conditions:

- Base system.
- System with a TCSC controller designed to eliminate the observed oscillation (HB) problems.
- System with an SSSC controller.
- System with an SVeC controller.

Figure 11 depicts the PV curves for the voltage magnitude at Bus 14 ("remote" load bus) for the various system conditions, under normal operating conditions and for a Line 2-4 outage (contingency case). A single loading parameter $\lambda$ is used to represent a uniform load and generation increase throughout the system with respect to the base load and generation as follows:

$$\begin{aligned} P_L &= \lambda P_{L0} \\ Q_L &= \lambda Q_{L0} \\ P_G &= (\lambda + K_G)\, P_{G0} \end{aligned} \tag{13}$$

where $\lambda$ is the loading factor in p.u.; $P_L$ and $Q_L$ represent the load powers; $P_G$ stands for the generators' output powers; and $K_G$ is a variable used to model a distributed slack bus, so that the losses are distributed according to the base output powers of the generators. Note that in this case only the generators at Buses 1 and 2 are assumed to supply the power associated with the load and loss changes.

As $\lambda$ increases, the system approaches an oscillatory instability (HB) point at $\lambda = 1.4$ p.u. for the base case, and $\lambda = 1.33$ p.u. for the contingency case, as illustrated in Fig.11. Observe that at a loading point $\lambda = 1.37$ p.u., which defines the operating point depicted in Fig.11, a Line 2-4 trip yields oscillatory stability problems for the assumed constant power load models, as demonstrated by the eigenvalue diagram shown in Fig.12 (the critical eigenvalues $0.1608 \pm j8.5075$ are related to the exciter mode of the generator at Bus 1), with a sustained oscillation appearing in the system.

To control (damp) the oscillations associated with the HB points depicted in Fig.11, the TCSC, SSSC and SVeC controllers described in Sections III and IV are individually added to Line 1-5. All controllers were rated at the same compensation level of 50%, and the controllers' parameters were chosen to obtain the same damping ratio at the same system and loading conditions. For this compensation level, the active power flowing through the line is increased and controlled from 107.5 MW to 181 MW.

Figure 13 shows the PV curves for the test system with each of the embedded controllers, for both the base case and the contingency case. Observe that the controllers increase the "dynamic" loadability of the system by increasing the loading conditions at which the HB appears to $\lambda = 1.6$ p.u. for the SSSC and TCSC, and $\lambda = 1.58$ p.u. for the SVeC. For the case of the Line 2-4 outage, no HBs are observed, with the maximum dynamic loadability of the system corresponding to its "static" one at $\lambda = 1.52$ p.u.

At a $\lambda = 1.37$ p.u. loading level, the damping ratio of 1.1% associated with the Line 2-4 trip improves to 4.5% with

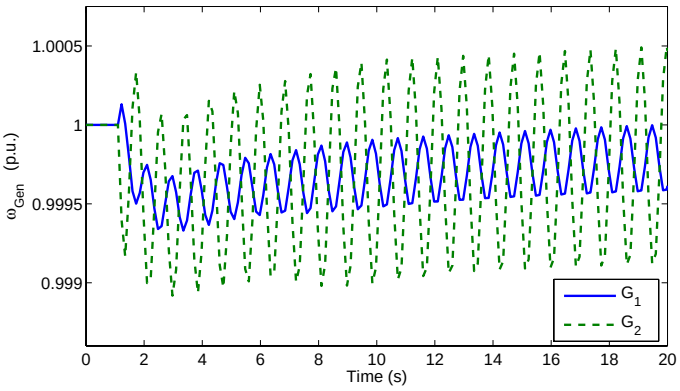


Fig. 14. Generators speed oscillation due to a Line 2-4 trip at $\lambda = 1.37$ p.u. for the 14-bus test system.

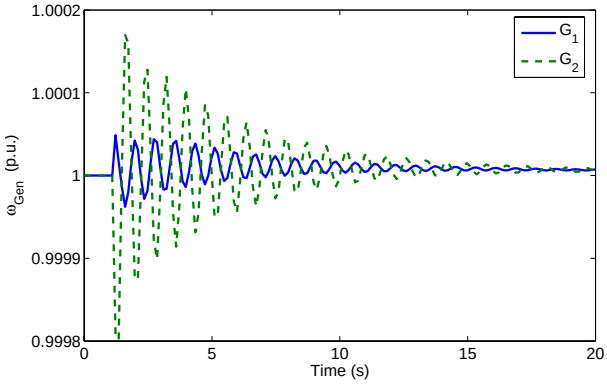


Fig. 15. Generators speed oscillation due to a Line 2-4 trip at $\lambda = 1.37$ p.u. for the 14-bus test system with SVeC.

the SVeC and TCSC, and 4.6% with the SSSC. All of this is confirmed through the time-domain simulations illustrated in Figs. 14-17, which show the 2 main generators' angular velocities for the 4 studied cases when the Line 2-4 is tripped at $t = 1$ s. All controllers were tuned at this loading level based on an eigenvalue analysis and a minimum target damping of 4%. These results show the effective damping of the sustained oscillations by all FACTS controllers under study, with the SVeC and TCSC performing quite similarly, and the SSSC showing slightly larger oscillations.

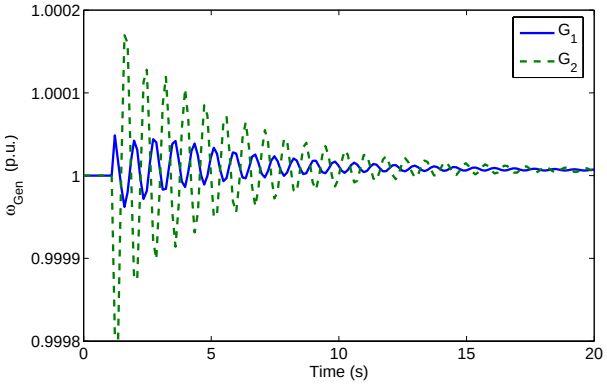


Fig. 16. Generators speed oscillation due to a Line 2-4 trip at $\lambda = 1.37$ p.u. for the 14-bus test system with TCSC.

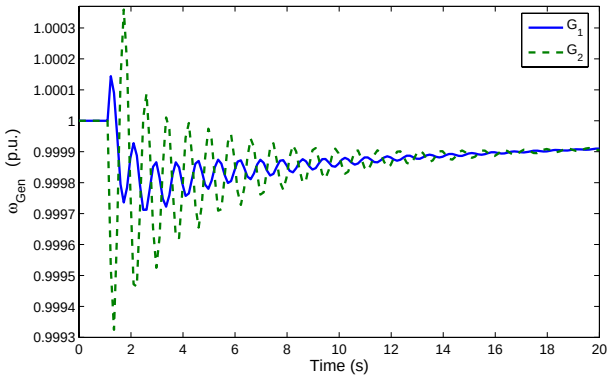


Fig. 17. Generators speed oscillation due to a Line 2-4 trip at $\lambda = 1.37$ p.u. for the 14-bus test system with SSSC.


Fig. 18. Schematic diagram of the Mexican power system.

### B. Mexican Power Grid Equivalent

The Mexican interconnected power system encompasses 7 regional systems, with a generation capacity in 2004 of 54 GW and an annual consumption level of 183.3 TWh in 2005. A schematic diagram of the full system is provided in Fig.18, showing the approximate geographical location of its four main control areas. The transmission grid comprises a large 400/230 kV system stretching from the southern border with Central America to its northern interconnections with the US. The north and south subsystems are characterized by long, sparsely interconnected transmission paths. The major load centers are concentrated on large metropolitan areas, mainly Mexico City in the central system, Guadalajara City in the western system, and Monterrey City in the northeastern system.

The studies presented here are based on a reduced model representing the northern, northeastern, western, central and southeastern areas of the system. This equivalent system consists of 190 buses, 265 400/230/138/115 kV transmission lines, 46 generators, and 90 loads modeled as constant power loads to simulate maximum system stress; in this model, no interconnections with the northwest are considered. A single-line diagram of the reduced model is shown in Fig.19. Buses 1-6 and 46 represent hydro generators in the southern

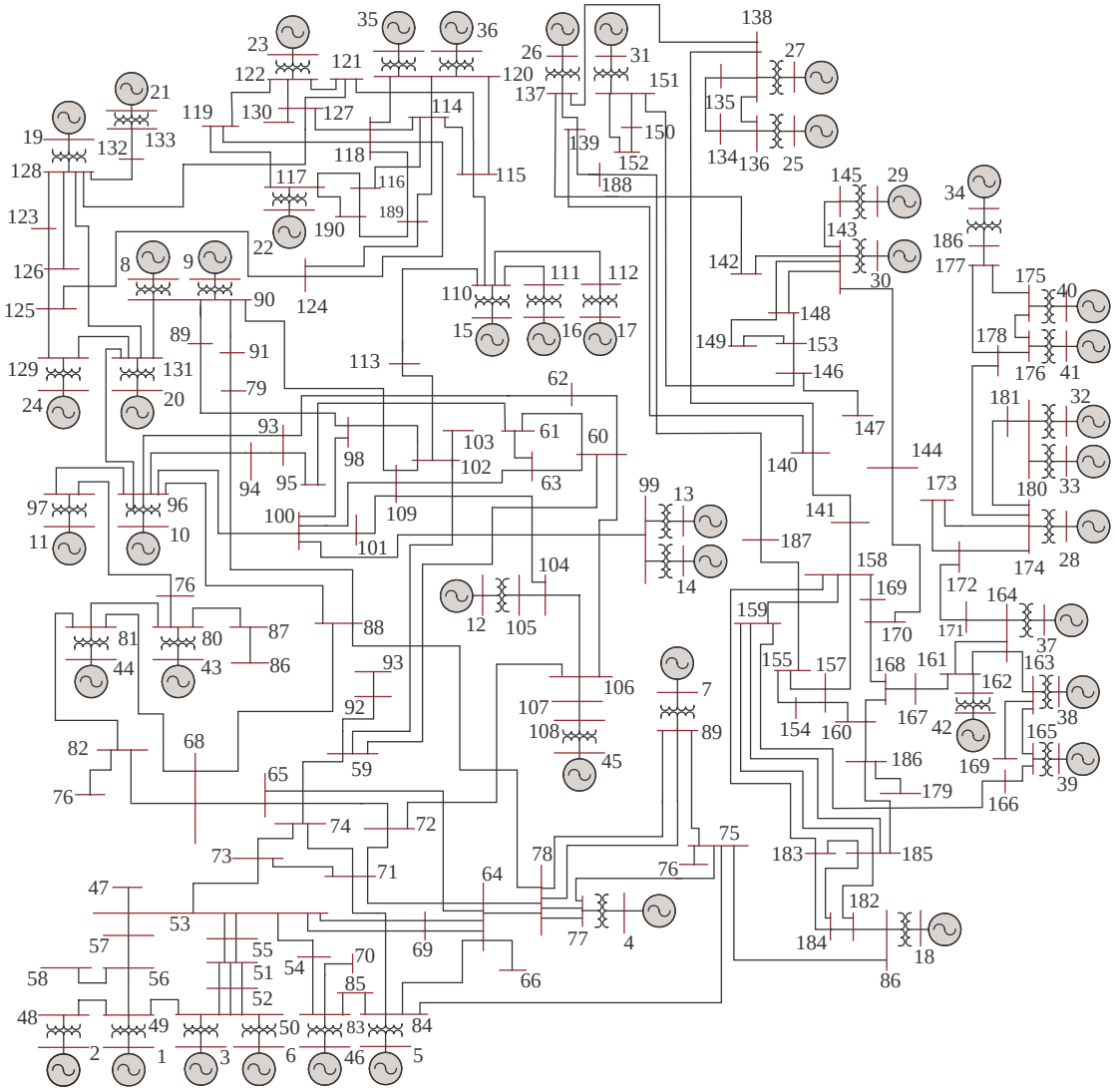

Fig. 19. Mexican power system 190-bus, 46-generator model.

peninsular subsystem; Bus 75 corresponds to Poza Rica, which interconnects the south with the northwest (Monterrey); the upper right hand side of the figure shows the main generators in the north; and the center and left of the figure correspond to the western and center parts of the country, representing mainly Guadalajara and Mexico City, respectively.

As in the case of the 14-bus test system, the results presented here correspond to the system without FACTS controllers and with a TCSC, an SSSC, and an SVeC controller, all introduced one at a time to eliminate oscillatory problems associated with an observed HB. Figure 20 depicts the PV curves of the power system in normal conditions and for a Line 53-73 outage (contingency). The system loading and generation is changed uniformly as in the case of the 14-bus test system, i.e. (13). As loading levels increase by increasing $\lambda$, the system approaches an oscillatory instability (HB point). Figure 21 shows the eigenvalues of the system for the base operating load ($\lambda = 1$ p.u.) and a Line 53-73 outage; in this case, the critical eigenvalues are related to the velocity and

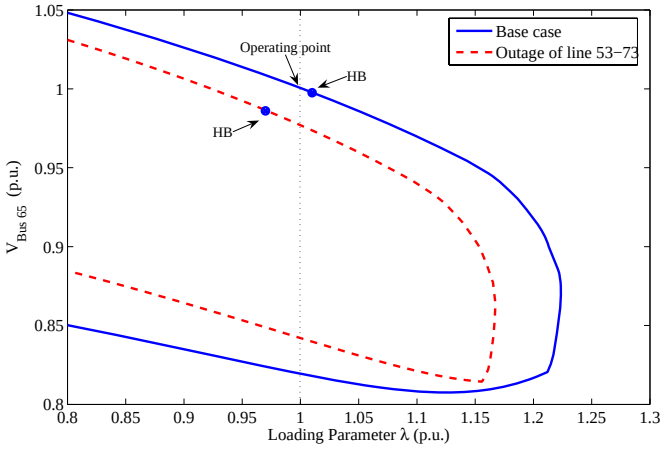


Fig. 20. PV curves and HB points for the Mexican system.

internal angle of the generator at Bus 1. It is important to highlight the fact that the oscillatory stabilities observed in this

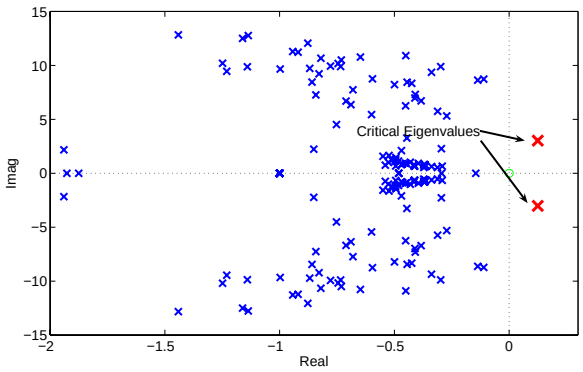


Fig. 21. Eigenvalues of the Mexican system at $\lambda = 1$ p.u. with an outage of Line 53-73.

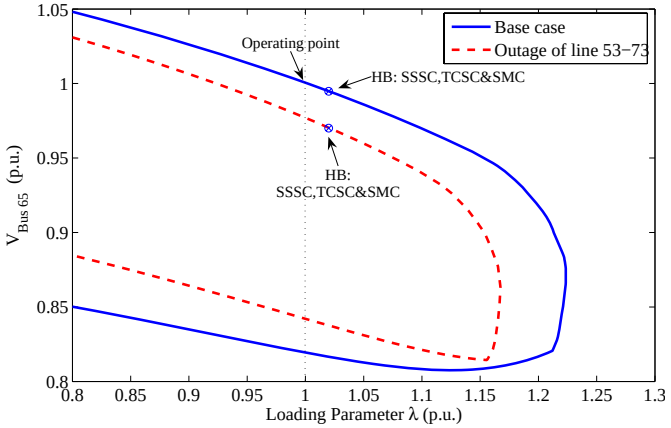


Fig. 22. PV curves for the Mexican system.

TABLE I
CRITICAL DAMPING RATIOS AND FREQUENCIES WITH FACTS CONTROLLERS AT DIFFERENT LOCATIONS FOR THE MEXICAN SYSTEM

| | SVeC | | TCSC | | SSSC | |
|---|---|---|---|---|---|---|
| Line | $f$ Hz | $\zeta$ % | $f$ Hz | $\zeta$ % | $f$ Hz | $\zeta$ % |
| 54-53 | 0.5936 | 0.8079 | 0.5936 | 0.8077 | 0.5932 | 0.7731 |
| **57-53** | **0.5759** | **3.2292** | **0.4766** | **1.5338** | **0.5854** | **2.7987** |
| 73-71 | 0.5741 | 0.6783 | 0.5861 | 0.6871 | 0.5872 | 0.7622 |
| 74-59 | 0.6113 | 0.8518 | 0.6193 | 0.3664 | 0.6018 | 0.8548 |
| 71-72 | 0.5914 | 0.7887 | 0.5915 | 0.7817 | 0.5901 | 0.8211 |
| 64-65 | 0.5916 | 0.7890 | 0.5922 | 0.7534 | 0.5883 | 0.8911 |

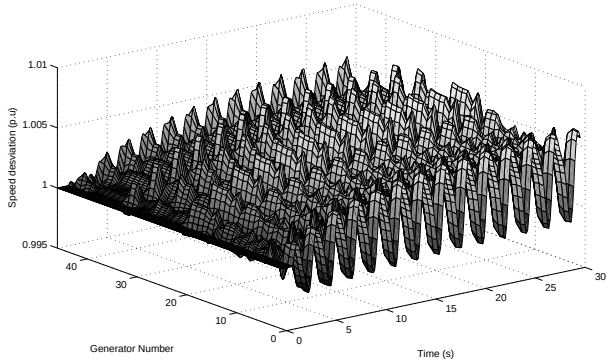


Fig. 23. Generators speed oscillation due to an outage of Line 53-73 at $\lambda = 1$ p.u.

case are due to the constant power load model used, which stresses the system more than other load models such as a constant impedance ones; no oscillatory problems are observed with a constant impedance model.

To find the best suitable location of the FACTS controllers under study for the removal of the oscillatory instability observed when the Line 53-73 is tripped, small-perturbation (eigenvalue) analyses were performed for the system with the line removed. In these studies, a 0.48 Hz unstable oscillatory mode with a damping ratio $\zeta = -1.4\%$ was observed at $\lambda = 1p.u.$, due to the speed and angle of the generator at Bus 1; this mode corresponds to an interaction between the south system against machines in the center, southeastern and peninsular systems. Table I shows the critical damping and frequency values obtained for several of the transmission lines considered as possible candidates for placement of an SVeC, TCSC or SSSC when the Line 53-73 is tripped. Observe that the best candidate location to prevent the HB problem is Line 57-53 (highlighted); this is confirmed through time-domain simulations. In this particular case, the SVeC shows a similar performance as the SSSC and better performance than the TCSC.

Figure 22 depicts the PV curves for the system with each of the FACTS controllers under study connected in series with Line 57-53 with a compensation level of 50%; in this case, the active power flowing through the line is increased and controlled from 815.27 MW to 924.13 MW. The controllers were tuned through an eigenvalue analysis at base loading conditions with Line 53-73 removed and a target damping of 3%; however, only the SVeC could be tuned to these specifications, with the other two controllers only providing the maximum damping shown in Table I, i.e. about 1.5% for the TCSC and 2.8% for the SSSC. (Note that it should possible to improve the damping ratios of the TSCS and SSSC controllers through the utilization of more sophisticated controllers as discussed for example in [15] for the TCSC.)

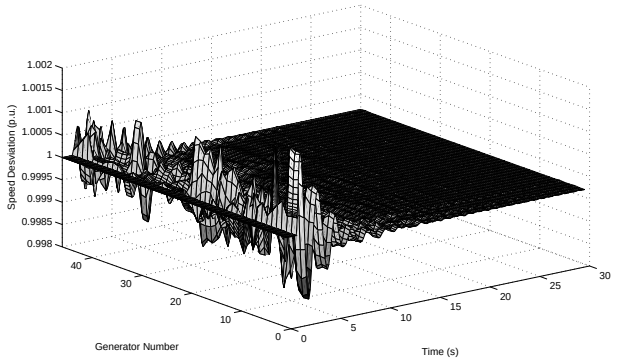


Fig. 24. Generators speed oscillation due to outage of Line 53-73 at $\lambda = 1$ p.u. with SVeC.

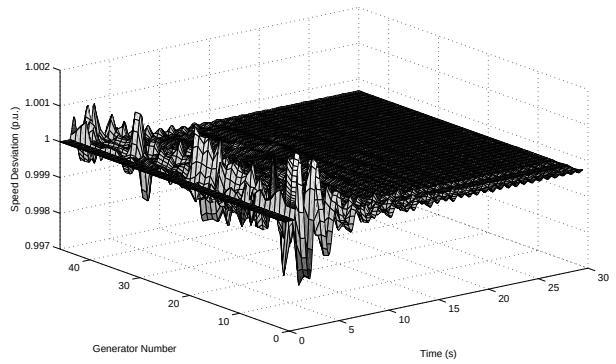


Fig. 25. Generators speed oscillation due to outage of Line 53-73 at $\lambda = 1$ p.u. with TCSC.

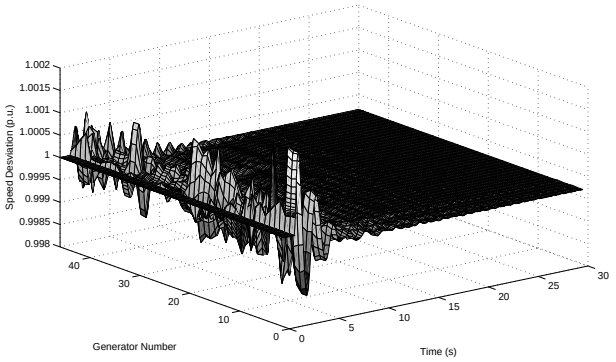


Fig. 26. Generators speed oscillation due to outage of Line 53-73 at $\lambda = 1$ p.u. with SSSC.

Observe that the controllers do not significantly affect the HB observed for the system without contingencies (base case), whereas the appearance of the oscillatory problem for the system without Line 53-73 conditions is moved to a higher loading condition (from $\lambda = 0.97p.u.$ to $1.02p.u.$); this is to be expected given that the latter are the system conditions used to place and tune the controllers. This is confirmed through the time-domain simulation results depicted in Figs. 23-26, where it can be observed that the SVeC and SSSC provide better damping for a Line 53-73 trip than the TCSC.

## VI. Conclusions

A simple stability model and controls based on the appropriate modulation of an equivalent series reactance of an SVeC were proposed and discussed in this paper. Full stability studies, i.e. voltage, small-perturbation and transient stability analyses were used to verify the impact of the SVeC in a multimachine power system. The performance of the SVeC with respect to similar series-connected FACTS controllers, namely TCSC and SSSC, were also presented. The results obtained for a couple of realistic test systems demonstrate the applicability of the controller and its ability to eliminate power oscillations triggered by system disturbances.

The results obtained demonstrate that the SVeC performs very similarly if not better than the TCSC and SSSC. Hence, it may be concluded that the SVeC is certainly a competitive, and in some cases better, option compared to current series-connected FACTS controllers, considering that the direct ac/ac power conversion principle of the SVeC leads to an overall more compact, simpler and durable controller, with no large dc-link energy storage components and a simpler PWM controller.

## References

[1] "Final Report on the August 14, 2003 blackout in the United States and Canada: Causes and recommendations," *U. S. - Canada Power System Outage Task Force*, April 2004.

[2] C. W. Taylor and D. C. Erickson "Recording and analyzing the July 2 cascading outage," *IEEE Computer Applications in Power*, vol. 10, Jan. 1997, pp. 26-30.

[3] N. G. Hingorani and L. Gyugyi, *Understanding FACTS: Concepts and Technology of Flexible AC Transmission Systems*, Piscataway, NJ: IEEE Press, 2000.

[4] L. Gyugyi, "Dynamic compensation of AC transmission lines by solid-state synchronous voltage sources," *IEEE Trans. Power Del.*, vol. 9, no. 2, pp. 904-911, Apr. 1994.

[5] L. Gyugyi, C. D. Schauder, S. L. Williams, T. R. Rietman, D. R. Torgerson, and A. Edris, "The unified power flow controller: A new approach to power transmission control," *IEEE Trans. Power Del.*, vol. 10, no. 2, pp. 1085-1097, Apr. 1995.

[6] L. Gyugyi, C. Schauder, and K. K. Sen, "Static synchronous series compensator: A solid-state approach to the series compensation of transmission lines," *IEEE Trans. Power Del.*, vol. 12, no. 1, pp. 406-417, Jan. 1997.

[7] K. K. Sen, "Static synchronous series compensator: Theory, modeling, and application," *IEEE Trans. Power Del.*, vol. 13, no. 1, pp. 241-246, Jan. 1998.

[8] C. D. Savelli, C. P. Pellanda, N. Martins, J. P. N. Macedo, A. A. Barbosa, and S. G. Luz, "Robust Signals for the TCSC Oscillation Damping Controllers of the Brazilian North-South Interconnection Considering Multiple Power Flow Scenarios and External Disturbances", *Proc. Power Engineering Society General Meeting*, Tampa, FL, June 2007.

[9] L. A. C. Lopes and G. Joos, "Pulse width modulated capacitor for series compensation," *IEEE Trans. Power Electron.*, vol. 16, no. 2, pp. 167-174, Mar. 2001.

[10] G. Venkataramanan and B. K. Johnson, "Pulse width modulated series compensator," *IEE Proc. Gen., Trans. and Dist.*, vol. 149, no. 1, pp. 71-75, Jan. 2002.

[11] G. Venkataramanan, "Three-phase vector switching converters for power flow control," *IEE Proc. Elect. Power Appl.*, vol. 151, no. 3, pp. 321-333, May 2004.

[12] F. Mancilla-David and G. Venkataramanan, "A pulse width modulated AC link unified power flow controller," in Proc. *IEEE Power Engineering Society General Meeting*, San Francisco, CA, vol. 2, pp. 1314-1321, July 2005.

[13] F. Z. Peng, L. Chen, and F. Zhang, "Simple topologies of PWM ac-ac converters," *IEEE Power Electron. Letters*, vol. 1, no. 1, pp. 10-13, March 2003.

[14] F. Mancilla-David, S. Bhattacharya, G. Venkataramanan, "A Comparative Evaluation of Series Power-Flow Controllers Using DC- and AC-Link Converters," *IEEE Trans. Power Del.*, vol. 23, no. 2, pp. 985-996, April 2008.

[15] V. Venkatasubramanian and C. W. Taylor, "Improving Pacific Intertie stability using Slatt thyristor controlled series compensation," in *Proc. PES Winter Meeting*, pp. 1468-1470, Jan. 2000.

[16] O. Simon, J. Mahlein, M. N. Muenzer, and M. Bruckmann, "Modern solutions for industrial matrix-converter applications," *IEEE Trans. Industrial Electronics*, vol. 49, no. 2, pp. 401-406, April 2002

[17] P. Wheeler, J. Clare, L. Empringham, M. Apap, and M. Bland, "Matrix converters," *Power Engineering Journal*, vol. 16, no. 6, pp. 273-282, Dec. 2002.

[18] J. M. Ramirez, J. M. Gonzalez, and M. L. Crow, "Steady state formulation of FACTS devices based on ac/ac converters," *IEE Proc. Electric Power Appl.*, vol. 1, no. 4, pp. 619-631, July 2007

[19] J. M.Gonzalez and J. M. Ramirez, "AC/AC series converter in transient stability," in *Proc. NAPS*, pp. 205-211, Las Cruces, New Mexico, Sept. 2007.

[20] J. M. Ramirez and J. M. Gonzalez, "Steady-state and transient stability studies with an ac-ac PWM series compensator," *IEEE-PES Summer Meeting*, Tampa, Florida, 2007.
[21] R. Seydel, *Practical Bifurcation and Stability Analysis: From Equilibrium to Chaos*, Second Edition, Springer-Verlag, New York, 1994.
[22] P. Kundur, *Power System Stability and Control*. McGraw Hill, New York, 1994.
[23] C. A. Cañizares, editor, "Voltage stability assessment: Concepts, practices and tools," *IEEE/PES Power System Stability Subcommittee*, Tech. Rep. SP101PSS, August 2002.
[24] D. J. Hill and I. M. Y. Mareels, "Stability theory for differential algebraic systems with application to power systems," *IEEE Trans. Circuits and Systems*, vol. 37, no. 11, pp. 1416-1423, Nov. 1990.
[25] N. Mithulananthan, "Hopf Bifurcation Control and Indices for Power System with Interacting Generator and FACTS Controllers," PhD thesis, University of Waterloo, Waterloo, ON, Canada, 2002. [Online]. Available: http://thunderbox.uwaterloo.ca/ claudio/thesis/mithulan
[26] C. A. Cañizares, F. L. Alvarado, C. L. DeMarco, I. Dobson, and W. F. Long, "Point of Collapse Methods Applied to AC/DC Power Systems," *IEEE Trans. Power Systems*, vol. 7, no. 2, May 1992, pp. 673-683.
[27] V. Ajjarapu and B. Lee, "Bifurcation theory and its application to nonlinear dynamical phenomena in power systems," *IEEE Trans. Power Systems*, vol. 7, no. 2, pp. 424-431, Feb. 1992.
[28] C. A. Cañizares and S. Hranilovic, "Transcritical and Hopf bifurcations in ac/dc systems," in *Proc. Bulk Power System Voltage Phenomena III-Voltage Stability and Security*, Davos, Switzerland, pp. 105-114, Aug. 1994.
[29] E. H. Abed and P.P. Varaiya, "Nonlinear oscillation in power systems," *Int. J. Electric Power and Energy Systems*, vol. 6, pp. 37-43, 1984.
[30] R. Mihalic and U. Gabrijel, "A structure-preserving energy function for a static series synchronous compensator," *IEEE Transactions on Power Systems*, vol. 19, no. 3, pp. 1501–1507, 2004.
[31] F. Milano, "Power System Analysis Toolbox: Documentation for PSAT version 2.0.0 $\beta$," March 2007.

**Juan Miguel González** obtained his BS in Electrical Engineering from Universidad de Colima, México in 2004, and MSc in Electrical Engineering from CINVESTAV, where he is pursuing a PhD degree. His primary area of interest is the modeling, simulation, analysis and control of FACTS devices.

**Claudio A. Cañizares** (S'85, M'91, SM'00, F'07) received in April 1984 the Electrical Engineer Diploma from the Escuela Politécnica Nacional, Quito-Ecuador, where he held different teaching and administrative positions from 1983 to 1993. His MS (1988) and PhD (1991) degrees in Electrical Engineering are from the University of Wisconsin-Madison. He has been at the University of Waterloo since 1993, where he is currently a Full Professor. His research activities concentrate on the study of modeling, simulation, control, stability, computational and dispatch issues in power systems in the context of competitive electricity markets.

**Juan M. Ramírez** obtained his BS in Electrical Engineering from Universidad de Guanajuato, México in 1984; MSc in Electrical Engineering from UNAM in 1987; and PhD in Electrical Engineering from UANL in 1992. He joined the department of Electrical Engineering of CINVESTAV in 1999, where he is currently a Full-time Professor. His areas of interest are in FACTS devices and control of electrical power systems.